Molecular Plant
Research Article

CellPress
PARTNER JOURNAL

Role of UDP-Glucuronic Acid Decarboxylase in Xylan Biosynthesis in *Arabidopsis*

Beiqing Kuang[1,2,9], Xianhai Zhao[1,2,9], Chun Zhou[1,2], Wei Zeng[3], Junli Ren[4], Berit Ebert[3], Cherie T. Beahan[3], Xiaomei Deng[2], Qingyin Zeng[5], Gongke Zhou[6], Monika S. Doblin[3], Joshua L. Heazlewood[3,7], Antony Bacic[3], Xiaoyang Chen[1,2,8,*] and Ai-Min Wu[1,2,8,*]

[1]State Key Laboratory for Conservation and Utilization of Subtropical Agro-bioresources, South China Agricultural University, Guangzhou 510642, China

[2]Guangdong Key Laboratory for Innovative Development and Utilization of Forest Plant Germplasm, College of Forestry and Landscape Architecture, South China Agricultural University, Guangzhou 510642, China

[3]ARC Centre of Excellence in Plant Cell Walls, School of BioSciences, The University of Melbourne, Parkville, VIC 3010, Australia

[4]State Key Laboratory of Pulp and Paper Engineering, South China University of Technology, Guangzhou 510640, China

[5]Institute of Botany, The Chinese Academy of Science, Beijing 100093, China

[6]Qingdao Institute of Bioenergy and Bioprocess Technology, Chinese Academy of Sciences, Qingdao 266101, China

[7]Joint BioEnergy Institute and Physical Biosciences Division, Lawrence Berkeley National Laboratory, Berkeley, CA 94720, USA

[8]Guangdong Province Research Center of woody forage engineering technology, Guangzhou, 510642, China

[9]These authors have contributed equally to this article.

***Correspondence: Xiaoyang Chen (xychen@scau.edu.cn), Ai-Min Wu (wuaimin@scau.edu.cn)**

http://dx.doi.org/10.1016/j.molp.2016.04.013

ABSTRACT

UDP-xylose (UDP-Xyl) is the Xyl donor used in the synthesis of major plant cell-wall polysaccharides such as xylan (as a backbone-chain monosaccharide) and xyloglucan (as a branching monosaccharide). The biosynthesis of UDP-Xyl from UDP-glucuronic acid (UDP-GlcA) is irreversibly catalyzed by UDP-glucuronic acid decarboxylase (UXS). Until now, little has been known about the physiological roles of UXS in plants. Here, we report that *AtUXS1*, *AtUXS2*, and *AtUXS4* are located in the Golgi apparatus whereas *AtUXS3*, *AtUXS5*, and *AtUXS6* are located in the cytosol. Although all six single *AtUXS* T-DNA mutants and the *uxs1 usx2 uxs4* triple mutant show no obvious phenotype, the *uxs3 uxs5 uxs6* triple mutant has an irregular xylem phenotype. Monosaccharide analysis showed that Xyl levels decreased in *uxs3 uxs5 uxs6* and linkage analysis confirmed that the xylan content in *uxs3 xus5 uxs6* declined, indicating that UDP-Xyl from cytosol AtUXS participates in xylan synthesis. Gel-permeation chromatography showed that the molecular weight of non-cellulosic polysaccharides in the triple mutants, mainly composed of xylans, is lower than that in the wild type, suggesting an effect on the elongation of the xylan backbone. Upon saccharification treatment stems of the *uxs3 uxs5 uxs6* triple mutants released monosaccharides with a higher efficiency than those of the wild type. Taken together, our results indicate that the cytosol UXS plays a more important role than the Golgi-localized UXS in xylan biosynthesis.

Key words: UDP-Xylose, xylan, UDP-Glucuronic acid decarboxylase, localization

Kuang B., Zhao X., Zhou C., Zeng W., Ren J., Ebert B., Beahan C.T., Deng X., Zeng Q., Zhou G., Doblin M.S., Heazlewood J.L., Bacic A., Chen X., and Wu A.-M. (2016). Role of UDP-Glucuronic Acid Decarboxylase in Xylan Biosynthesis in *Arabidopsis*. Mol. Plant. **9**, 1119–1131.

INTRODUCTION

Plant cell-wall polysaccharides consist of cellulose and non-cellulosic polysaccharides and are a major source of renewable biomass. They play important roles in cellular growth and differentiation, and plant morphology and architecture, as well as providing an energy reserve (Doblin et al., 2010; Pauly and Keegstra, 2010). In general, plants utilize sunlight to convert H_2O and CO_2 into sugars in the chloroplast. These sugars pass through a series of enzyme-catalyzed pathways, including nucleotide sugar metabolism, and accumulate as starch and sucrose in fruits and tubers as well as in cell-wall polysaccharides and glycoproteins (Okazawa et al., 1993; Reiter and Vanzin, 2001; Seifert, 2004). The activated sugar donors of cell-wall polysaccharides are nucleoside diphosphate

Published by the Molecular Plant Shanghai Editorial Office in association with Cell Press, an imprint of Elsevier Inc., on behalf of CSPB and IPPE, SIBS, CAS.

(NDP) sugars, including UDP-D-glucose (UDP-Glc), UDP-D-glucuronate (UDP-GlcA), UDP-D-xylose (UDP-Xyl), UDP-D-galactose (UDP-Gal), UDP-D-galacturonate (UDP-GalA), UDP-D-apiose (UDP-Api), UDP-L-arabinose (UDP-Ara) UDP-L-rhamnose (UDP-Rha), and GDP-D-mannose (GDP-Man) (Reiter, 2008).

UDP-Xyl is an essential glycosyl donor required for the biosynthesis of heteroxylans and xyloglucans (Ray, 1980; Hayashi et al., 1988; Rodgers and Bolwell, 1992; Reiter, 2008) and for the side chains of two types of pectin, xylogalacturonan and rhamnogalacturonan II (RG-II). In addition, UDP-Xyl is the donor for glycoprotein, proteoglycan, and glycolipid synthesis (Gotting et al., 2000; Strasser et al., 2000; Seifert, 2004). Mutant analyses suggest that *IRX9*, *IRX10*, and *IRX14* and their homologs encode enzymes responsible for xylan assembly (Brown et al., 2007, 2009; Lee et al., 2007; Peña et al., 2007; Wu et al., 2009, 2010). Lee et al. (2012) demonstrated that co-expression of IRX9 and IRX14 in tobacco BY2 cells exhibited xylosyltransferase (XylT) activity, but expression of either IRX9 or IRX14 alone resulted in no activity. Recently, two research groups have independently demonstrated that heterologously expressed IRX10 displayed xylan XylT activity in a processive mode. Urbanowicz et al. (2014) expressed *Arabidopsis IRX10-L* in mammalian HEK293 cells and Jensen et al. (2014) expressed separately *Arabidopsis*, psyllium (*Plantago ovata*) and moss (*Physcomitrella patens*) *IRX10* gene in *Pichia pastoris*, finding that all of the heterologously expressed IRX10 proteins were able to add multiple Xyl residues onto a xylo-oligosaccharide acceptor. In addition, *XXT1*, *XXT2*, and *XXT5* encode XylTs that are required for xyloglucan side-chain biosynthesis (Cavalier and Keegstra, 2006; Cavalier et al., 2008; Zabotina et al., 2008). *RGXT1* and *RGXT2* encode XylTs involved in the synthesis of RG-II side chains and *XGD1* is involved in xylogalacturonan synthesis (Egelund et al., 2006; Jensen et al., 2008). In plants, UDP-Xyl can be epimerized by UDP-Xyl 4-epimerases (UXE, EC 5.1.3.5) to UDP-Ara, which is used for arabinoxylan and pectin biosynthesis (Reiter and Vanzin, 2001). Thus, given the central role of UDP-Xyl in polysaccharide and glycoprotein biosynthesis, it is vital to elucidate the mechanism underlying its synthesis.

UDP-glucuronic acid decarboxylase (UXS) irreversibly catalyzes decarboxylation of UDP-glucuronic acid (UDP-GlcA) to form UDP-Xyl (Bar-Peled et al., 2001; Harper and Bar-Peled, 2002). The first *UXS* gene was identified from the fungus *Cryptococcus neoformans* based on sequence homology with the bacterial *ORF3* gene (*arnA*), which was hypothesized to exhibit a similar function (Bar-Peled et al., 2001). The first plant *UXS* genes were identified in *Arabidopsis* by sequence homology to the *C. neoformans UXS* gene (Harper and Bar-Peled, 2002). Subsequently, *UXS* genes have been cloned from other plant species, including rice (*Oryza sativa*) (Suzuki et al., 2004), barley (*Hordeum vulgare*) (Zhang et al., 2005), tobacco (*Nicotiana tabacum*) (Bindschedler et al., 2007), and Chinese white poplar (*Populus tomentosa*) (Du et al., 2013).

Previous UXS studies have mainly focused on protein expression and enzyme activities (Harper and Bar-Peled, 2002; Kobayashi et al., 2002; Suzuki et al., 2003). In plants, UXS proteins are located in the cytosol or the Golgi/ER lumen (Harper and Bar-Peled, 2002; Kobayashi et al., 2002). Bioinformatic analyses of the UXS gene sequences predict that AtUXS1, AtUXS2, and AtUXS4 have a type II transmembrane domain, whereas AtUXS3, AtUXS5 and AtUXS6 are predicted to be cytosolic (Harper and Bar-Peled, 2002). This raises questions as to the function(s) of these two groups of AtUXS enzymes *in planta*.

To date almost all nucleotide sugar biosynthesis genes from plants have been cloned and expressed, and their catalytic activities have been established *in vitro*. In contrast, only a small number of these genes have been studied using molecular genetics techniques (Bar-Peled and O'Neill, 2011). In this study, we used reverse genetics and biochemistry approaches to analyze the functions of all six *Arabidopsis* UXS isoforms. Our results showed that the cytosol UXS play a more important role than the Golgi-localized UXS in xylan biosynthesis.

RESULTS

Phylogenetic Characteristics and Gene-Expression Analysis of *AtUXS* Genes

To understand the evolutionary history of the *UXS* gene family in land plants, we constructed a phylogenetic tree using 39 UXS protein sequences from *Arabidopsis thaliana* (At), *Chlamydomonas reinhardtii* (Cr), *Selaginella moellendorffii* (Sm), *P. patens* (Pp), *Picea abies* (Norway spruce; Ns), *Populus trichocarpa* (Pt), *Eucalyptus grandis* (Eg), *O. sativa* (Os), and *H. vulgare* (Hv) (Supplemental Table 1). The phylogenetic tree shows that *UXS* genes in land plants fall into two groups (groups I and II, Supplemental Figure 1). Based on predicted transmembrane structures by TMHMM2.0 (http://www.cbs.dtu.dk/services/TMHMM/, AtUXS proteins of Supplemental Figure 2 as example), all group I UXS proteins are devoid of transmembrane helices, whereas most of the group II UXS proteins contain a transmembrane helix.

There are six *AtUXS* genes encoding polypeptides of between 343 and 458 amino acids in *Arabidopsis*. Group I includes AtUXS3, AtUXS5, and AtUXS6 with 92.0% amino acid identity and group II includes AtUXS1, AtUXS2, and AtUXS4 with 76% amino acid identity (Supplemental Figure 3). All six proteins contain conserved features of the UXS family, including an N-terminal ADP-binding sequence GxxGxxG related to NAD(P) binding and a catalytic triad of Ser, Tyr, and Lys where the Tyr and Lys are in the conserved YxxxK motif (Wierenga et al., 1986; Harper and Bar-Peled, 2002). Group I proteins have the conserved amino acid sequence GGAGFVG whereas group II proteins have the conserved amino acid sequence GGAGFIG in the NAD(P)-binding site (Supplemental Figure 3).

Quantitative PCR (qPCR) was employed to determine developmental and spatial gene-expression levels of *AtUXS* genes in various organs (see Supplemental Table 2 for primers). The results showed that all six genes are most highly expressed in the stem, which is consistent with microarray data from *Arabidopsis* (Winter et al., 2007). In general, gene-expression levels in the group I clade (*AtUXS3*, *AtUXS5*, and *AtUXS6*) were higher than those in the group II clade (*AtUXS1*, *AtUXS2*, and *AtUXS4*), with *AtUXS1* and *AtUXS2* exhibiting the lowest expression levels among all six genes (Supplemental Figure 4). In addition, to compare *AtUXS* expression patterns with UDP-Xyl utilization, we undertook expression analysis of *IRX9* and

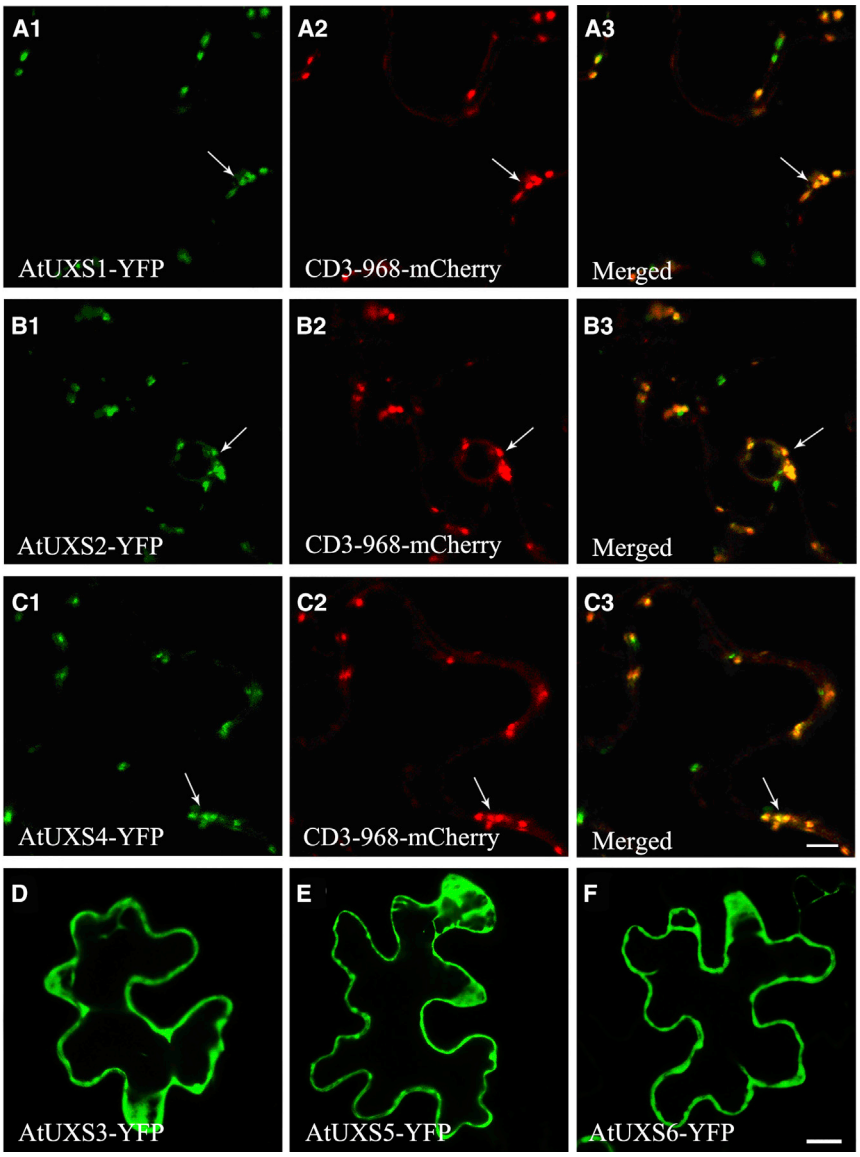

Figure 1. Subcellular Localization of AtUXS Proteins.

(A–F) C-terminal YFP fusions with individual *AtUXS* genes were expressed in *N. benthamiana*. UXS1-YFP, UXS2-YFP, and UXS4-YFP images are shown in **(A1)**, **(B1)**, and **(C1)**, respectively. Golgi-localized CD3-968-mCherry images are shown in **(A2)**, **(B2)**, and **(C2)**, and the merged images are shown in **(A3)**, **(B3)**, and **(C3)**, respectively. The arrows indicate the overlapped fluorescence. Confocal images from **(D)** to **(F)** are AtUXS3-YFP, AtUXS5-YFP, and AtUXS6-YFP, respectively. Scale bars represent 5 μm for **(A1)** to **(C3)** and 10 μm for **(D)** to **(F)**.

IRX10 (genes involved in xylan synthesis). Highest expression of these genes was also observed in stem tissue, similarly to *UXS3* and *UXS6* (Supplemental Figure 4B).

Subcellular Location of AtUXS Proteins

To experimentally verify the subcellular localization of AtUXS proteins, we transformed *Arabidopsis* plants with each AtUXS isoform fused to the yellow fluorescent protein (YFP) at the C terminus under the control of the cauliflower mosaic virus (CaMV) 35S promoter (P35S). AtUXS1, AtUXS2, and AtUXS4 are each predicted to contain a single transmembrane domain near the N terminus (amino acid residues 48–65, 44–61, and 44–61, respectively), indicating a type II membrane protein topology. The fluorescent signals of AtUXS1-, AtUXS2-, and AtUXS4-YFP were localized to small punctate bodies that resemble the Golgi (Supplemental Figure 5A–5C). In contrast, AtUXS3, AtUXS5, and AtUXS6 did not have predicted transmembrane domains, suggesting they are soluble cytoplasmic proteins. The signals for AtUXS3-, AtUXS5-, and AtUXS6-YFP were diffuse and evenly distributed throughout the cytoplasm (Supplemental Figure 5D–5F). To further confirm these findings, we performed heterologous expression of the same constructs in *N. benthamiana* leaves with a Golgi marker (G-rb CD3-968 mCherry) (Nelson et al., 2007). YFP fluorescent signals from AtUXS1, AtUXS2, and AtUXS4 were observed and found to co-localize with mCherry signals from CD3-968 in the Golgi apparatus (Figure 1A–1C). In contrast, fluorescent signals from AtUXS3, AtUXS5, and AtUXS6 were diffuse and found throughout the cytoplasm, which was most apparent at the cell peripheries due to the large vacuole (Figure 1D–1F). Taken together, these results indicate that AtUXS1, AtUXS2, and AtUXS4 are Golgi located, whereas AtUXS3, AtUXS5, and AtUXS6 are cytosolic.

The Catalytic Activity of AtUXS *In Vitro* and *In Planta*

In previous studies, AtUXS1, AtUXS2, and AtUXS3 were expressed in *Escherichia coli* and the N-terminally truncated forms of AtUXS1 and AtUXS2 showed low decarboxylase activities (Bar-Peled et al., 2001; Pattathil et al., 2005). To avoid difficulties in comparing membrane-bound and soluble proteins, we selected only the soluble AtUXS isoforms AtUXS3, AtUXS5, and AtUXS6 for expression in *E. coli* to compare catalytic properties. Full-length coding regions of *AtUXS3*, *AtUXS5*, and *AtUXS6* were cloned into the expression vector pGEX-4T (GE Healthcare), expressed in *E. coli*, and purified using the glutathione S-transferase (GST) tag (Supplemental Figure 6).

After incubation of recombinant AtUXS3, AtUXS5, and AtUXS6 proteins with the substrate UDP-GlcA, the reaction products were separated using high-performance liquid chromatography (HPLC). As predicted, the three AtUXS proteins catalyzed UDP-GlcA conversion to a new product (Supplemental Figure 7A), which had the same retention time as the UDP-Xyl standard. ^{1}H-nuclear magnetic resonance analysis confirmed that the product was UDP-Xyl (Supplemental Figure 7B). These results demonstrated that AtUXS3, AtUXS5, and AtUXS6 are functional

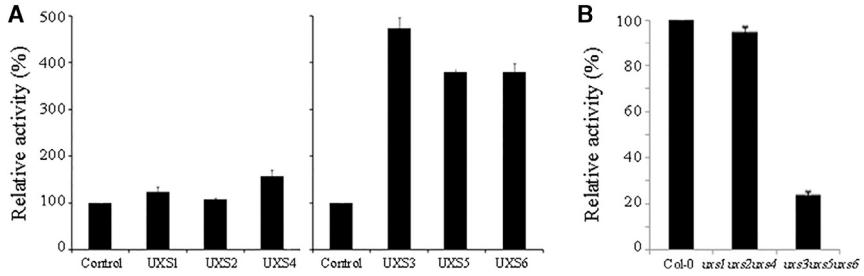

Figure 2. The Activities of AtUXS1-6 Heterologously Expressed in *N. benthamiana*.
Total tobacco proteins were extracted from 3-day-old inoculated tobacco leaves and their UXS activity for conversion of UDP-GlcA to UDP-Xyl measured.
(A) Heterologously expressed UXS activity was measured by the conversion rate of UDP-GlcA to UDP-Xyl, and the control injected with empty vector was set as 100%.
(B) The relative activities of UXS in the wild-type, *uxs1 uxs2 uxs4* (group II), and *uxs3 uxs5 uxs6* (group I) mutant extracts was determined. Total protein was extracted from 2-week-old plants growing in Murashige–Skoog medium. The mean of three biological replicates ± SE are shown.

UDP-GlcA decarboxylases. As stated earlier, AtUXS3, AtUXS5, and AtUXS6 share over 90% amino acid identity (Supplemental Figure 3) and a comparison of their kinetic parameters revealed different affinity capabilities with UDP-GlcA among AtUXS5 (K_m = 0.40 mM), AtUXS3 (K_m = 0.48 mM), and AtUXS6 (K_m = 0.54 mM) (Supplemental Figure 7C). The pH and temperature optima for all three isoforms were pH 6.0 (Supplemental Figure 7D) and 30°C (Supplemental Figure 7E), respectively, consistent with previously reported values (Harper and Bar-Peled, 2002).

To avoid technical difficulties associated with the handling of heterologously expressed transmembrane proteins in microorganisms, we used a plant-based heterologous protein expression system (*N. benthamiana*) to confirm AtUXS activity *in planta* (Jensen et al., 2008). The AtUXS5 polyclonal antibody and hemagglutinin (HA)-tag antibody were used together to assess protein expression levels in group I (soluble proteins) and group II (microsomal proteins), respectively. For each total protein extract from *N. benthamiana* leaves, similar western blot signals at a molecular weight of about 40 kDa were observed with the AtUXS5 antibody for all three group I UXS samples (Supplemental Figure 8). A similar result at a molecular weight of about 55 kDa was obtained when the group II UXS samples were probed with the HA antibody, indicating AtUXS protein activity could be compared independently in each group (Supplemental Figure 8). The AtUXS proteins from the two groups have different capacities to catalyze the conversion of UDP-GlcA to UDP-Xyl (Figure 2A). The heterologously expressed AtUXS proteins from group I resulted in a significant increase compared with control (empty vector) in enzyme activity, with the cytosolic-localized AtUXS3 showing the highest activity (475 nmol UDP-Xyl min^{-1} mg^{-1}). The Golgi-localized AtUXS proteins (group II) resulted in minimal activity compared with the control, with AtUXS2 having the lowest activity (53 nmol UDP-Xyl min^{-1} mg^{-1}) in group II (Figure 2A).

Multiple *UXS* Genes Are Redundant

The two different subcellular locations of the AtUXS isoforms raise a question of functional redundancy for these two groups in wall formation. As most non-cellulosic polysaccharides are synthesized in the Golgi lumen, do the Golgi-located AtUXS isoforms play a more important role in cell-wall polysaccharide formation than the cytosolic AtUXS isoforms? To investigate the role of the two groups of AtUXS *in vivo*, a reverse genetics approach was used. Seeds from existing T-DNA insertion lines for each *UXS* gene were obtained and the resultant seedlings genotyped to select homozygous individuals for further analysis (Figure 3A and Supplemental Table 3). To determine whether there was any residual expression of the T-DNA-tagged *UXS* genes, we used an RT–PCR approach with primers spanning the T-DNA insertion site. Our results showed that *uxs1* and *uxs5* are knockdown T-DNA lines, but all others were confirmed to be knockout lines (Figure 3B and Supplemental Table 4). None of the six single *uxs* mutants showed any obvious phenotype. Phenotype of rosette leaves, stem, flowers, and fertility were found to be similar to those of Col-0 plants (Supplemental Figure 9).

To overcome possible functional redundancy between the *UXS* genes, we preferentially generated double and triple mutant combinations of the group I and II genes. Although the double mutants maintained wild-type phenotypes (Supplemental Figure 9), the triple mutant *uxs3 uxs5 uxs6* (group I) exhibited delayed growth, a darker leaf color, shorter stems, and smaller flowers under long day conditions (16 h light/8 h dark) (Figure 3C and 3D). In contrast, the triple mutant *uxs1 uxs2 uxs4* (group II) displayed a less severe phenotype than *uxs3 uxs5 uxs6* (group I) and was more similar to the wild type (Figure 3C and 3D).

UXS enzyme activity in whole-cell extracts was measured between the two triple mutant lines and wild type. Approximately 65% of the wild-type level of UXS activity was observed in *uxs1 uxs2 uxs4* (group II) whereas *uxs3 uxs5 uxs6* (group I) only retained 25% of wild-type UXS activity (Figure 2B). These results suggest that the cytosolic AtUXS isoforms might supply a larger fraction of the UDP-Xyl pool and therefore may be more essential for plant growth.

Secondary Cell Walls Are Decreased in the UXS Triple Mutants

To explore whether the various observed phenotypes were caused by a defect in secondary cell walls, we examined transverse sections of stems for each mutant line by light and transmission electron microscopy. None of the six single *uxs* mutants showed abnormal morphologies (Supplemental Figure 10). Similarly, the *uxs1 uxs2 uxs4* mutant displayed normal vascular bundle morphology. However, a striking phenotype was observed in the stems of *uxs3 uxs5 uxs6* triple mutant, where a collapse of xylem vessels and reduced thickness of fiber cells and xylem vessel

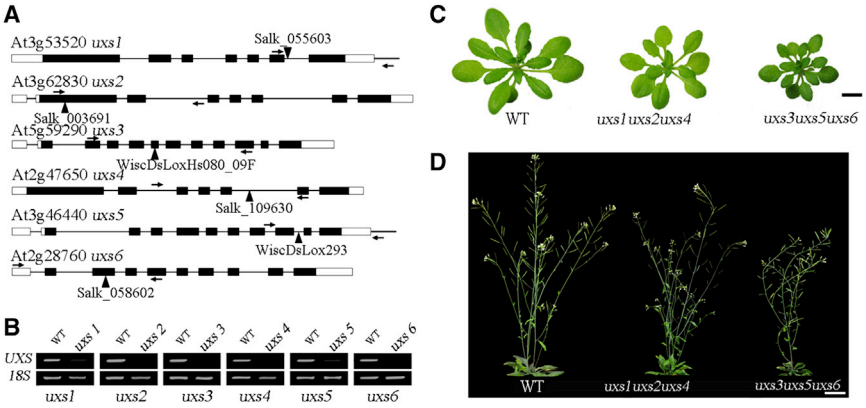

Figure 3. T-DNA Insertion Lines for the Six *Arabidopsis UXS* Genes and Mutant Plant Phenotypes.

(A) Intron–exon structure of *UXS* genes and location of T-DNA insertion in mutant alleles (triangles). Boxes represent exons and lines introns. *uxs1*, *uxs2*, *uxs3*, *uxs4*, *uxs5*, and *uxs6* have a T-DNA insertion in At3g53520, At3g62830, At5g59290, At2g47650, At3g46440, and At2g28760 loci, respectively. Arrows indicate the RT-PCR primer sites.

(B) RT–PCR analysis reveals no transcript in lines of *uxs2*, *uxs3*, *uxs4*, and *uxs6* mutants and reduced transcript in *uxs1* and *uxs5* compared with the wild type (WT) (Col-0). 18S ribosomal PCR results were used as the loading control. A total of three biological replicates were analyzed for each line. The primers used for RT–PCR are outlined in Supplemental Table 4.

(C) Five-week-old rosette leaves of wild-type Col-0, *uxs1uxs2uxs4*, and *uxs3uxs5uxs6* triple mutant plants. Scale bar represents 1 cm.

(D) Eight-week-old plants of wild-type Col-0, *uxs1uxs2uxs4*, and *uxs3uxs5uxs6* triple mutants. Scale bar represents 2 cm.

walls occurred when compared with the wild-type (Figure 4A–4F). The thickness of interfascicular fiber cell walls of the *uxs3 uxs5 uxs6* mutant was only 0.80 μm compared with the wild type (1.74 μm) and the *uxs1 uxs2 uxs4* mutant (1.34 μm) (Figure 4G–4I). The *uxs3 uxs5 uxs6* phenotype is reminiscent of the irregular xylem (*irx*) phenotype, suggesting that xylan synthesis in this mutant is severely affected (Brown et al., 2005).

Cell-Wall Composition in *uxs* Mutants

To examine the effect of *uxs* mutations on the cell wall, we determined the non-cellulosic monosaccharide composition of alcohol-insoluble residue (AIR) from stem material of the wild type and triple mutants. We observed minimal differences in the monosaccharide composition of stem material between the wild type and *uxs1 uxs2 uxs4* (group II) mutant (Table 1). In contrast, the levels of Xyl in cell-wall extracts from the *uxs3 uxs5 uxs6* (Group I) mutant were significantly lower, exhibiting a 21% decrease. We also observed a significant decrease in GlcA levels (42%) in the *uxs3 uxs5 uxs6* triple mutant as well as a two-fold increase in the amount of Ara (Table 1). These data indicated that cytosolic UXS is important for the biosynthesis of Xyl- and GlcA-containing cell-wall polysaccharides. These findings are consistent with the recent characterization of a UDP-Xyl transporter (UXT) transferring UDP-Xyl from the cytoplasm into the Golgi lumen for xylan biosynthesis (Ebert et al., 2015).

AIR from the inflorescence stems was also subjected to linkage analysis to assess polysaccharide composition in the triple mutants (Supplemental Table 5). The predominant polysaccharides in the cell walls from stem material were cellulose and heteroxylans with low amounts of heteromannans, xyloglucans, and pectic polysaccharides (Supplemental Table 5). Heteroxylan content decreased by approximately 30% in *uxs3 uxs5 uxs6* (group I) mutant stems (17.4 mol%) compared with the wild type (25.1 mol%). As expected, no obvious change was observed in heteroxylan content in the *uxs1 uxs2 uxs4* (group II) triple mutant. Cellulose content decreased in both *uxs1 uxs2 uxs4* and *uxs3 uxs5 uxs6* triple mutants, while the level of xyloglucan in both mutants showed no significant difference in the stem material compared with the wild type (Supplemental Table 5). Finally, the content of pectic polysaccharides approximately doubled in both the mutants (from 7.6 [wild-type] to 17.7 [*uxs1 uxs2 uxs4*] and 19.8 [*uxs3 uxs5 uxs6*] mol%, respectively), showing pleiotropic effects as previously observed when there have been attempts to modify the composition of plant cell walls (Doblin et al., 2014). The results indicate that cytosolic UXS might affect heteroxylan biosynthesis by regulating UDP-Xyl substrate concentrations.

The LM10 monoclonal antibody (McCartney et al., 2005) was used to investigate heteroxylan distribution in mutant stems. In wild-type plants, the strongest fluorescence signals were detected in the cell walls of xylem cells and interfascicular fibers. Weaker signals were detected in the *uxs3 uxs5 uxs6* triple mutant with this probe (Supplemental Figure 11). This result corroborates our linkage analysis, indicating that *uxs3 uxs5 uxs6* deposits less xylan in the stem compared with the wild type.

Xylan Structure Analysis in Triple *uxs* Mutants

In most xylan-related mutants such as *irx9*, *irx10*, and *irx14*, an increase in the proportion of MeGlcA to GlcA is observed (Brown et al., 2007, 2009; Lee et al., 2007; Peña et al., 2007; Wu et al., 2009, 2010). Therefore, the levels of GlcA and MeGlcA, which constitute the major side chain on *Arabidopsis* xylan, were analyzed in the wild type and the *uxs1 uxs2 uxs4* and *uxs3 uxs5 uxs6* triple mutants. Matrix-assisted laser desorption ionization time-of-flight mass spectrometry (MALDI-TOF MS) spectra showed the expected prominent pseudo-molecular ion peaks (*m/z*) of 745, 759, 767, 781 and 797 could be attributed to GlcA-Xyl_4-Na^+, MeGlcA-Xyl_4-Na^+, Gal-GlcA-Xyl_3-Na^+, GlcA-Xyl_4-$2Na^+$, MeGlcA-Xyl_4-$2Na^+$, and Gal-GlcA-Xyl_3-$2Na^+$ (Zhong et al., 2005, 2014), respectively. Comparing the peak areas of the pseudo-molecular ions MeGlcA/(MeGlcA + GlcA) in *uxs1 uxs2 uxs4* and *uxs3 uxs5 uxs6*, the proportion was determined to be 87.9% and 96.1%, respectively, showing an increase of 8.8% and 17.0%, respectively, compared with the wild type (79.1%) (Figure 5). The Gal-GlcA-Xyl_3 pseudo-molecular ions only represent a small proportion of the total measured GlcA and were therefore not considered. These data indicated that

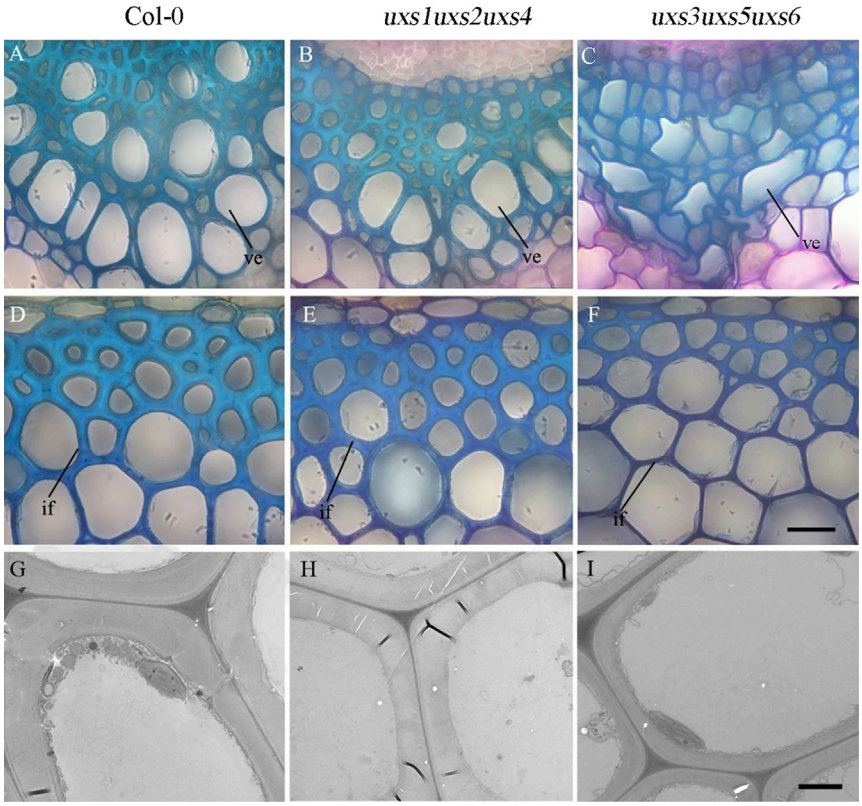

Figure 4. Vessel Morphology and Thickness of Secondary Cell Walls from the wild-type Col-0, *uxs1uxs2uxs4*, and *uxs3uxs5uxs6* Triple Mutants.

(A–C) Transverse sections of stems of the wild-type Col-0, *uxs1 uxs2 uxs4*, and *uxs3 uxs5 uxs6* triple mutants. Misshapen vessels in *uxs3 uxs5 uxs6* are apparent.

(D–F) Transverse sections of the interfascicular fiber region from the wild-type Col-0, *uxs1 uxs2 uxs4*, and *uxs3 uxs5 uxs6* triple mutants , showing reduced thickness in *uxs3uxs5uxs6*.

(G–I) Transmission electron micrographs of the interfascicular fiber region from the wild-type Col-0, *uxs1 uxs2 uxs4*, and *uxs3 uxs5 uxs6* triple mutants.

ve, vessel; if, interfascicular fibers. Scale bars represent 10 μm in **(A)** to **(F)** and 3 μm in **(G)** to **(I)**.

the *uxs* triple mutants respond in a manner similar to that of the xylan-related *irx* mutants.

Molecular Weight of Non-cellulosic Polysaccharide in *uxs* Triple Mutants

Our data have shown that there is a discernible reduction in xylan content in the *uxs3 uxs5 uxs6* triple mutant (Supplemental Table 5). Thus, we examined whether the molecular size distribution of the non-cellulosic polysaccharides, which is mainly xylan in the stem, was also affected in the *uxs* triple mutants. The molecular weight of non-cellulosic polysaccharide fractions from the wild type and *uxs1 uxs2 uxs4* and *uxs3 uxs5 uxs6* triple mutants were analyzed by gel-permeation chromatography (GPC) of extracted fractions in 1 N and 2 N KOH. A significant decrease in molecular weight was found in both triple mutants (Table 2). For non-cellulosic polysaccharides extracted in 1 N KOH, the weight-average molecular weight (M_w) and number-average molecular weight (M_n) of non-cellulosic polysaccharides in the *uxs3 uxs5 uxs6* mutant was 24.3 kDa and 9.7 kDa, respectively, both of which were significantly reduced compared with the wild type (Table 2). An intermediate M_w value between the wild type and *uxs3 uxs5 uxs6* was observed in *uxs1 uxs2 uxs4*. M_w values are higher for all three lines in the 2 N KOH extracted fractions, with *uxs1 uxs2 uxs4* and *uxs3 uxs5 uxs6* showing a similar M_w reduction trend compared with the wild type. However, all three lines have similar M_n values in 2 N KOH compared with 1 N KOH fractions, in which both mutants displayed reduced values compared with wild-type. The results indicated that the non-cellulosic polysaccharide backbone length is significantly reduced in both the *uxs* triple mutants, with *uxs3 uxs5 uxs6* having the greater size reduction in the two mutants.

The *uxs* Triple Mutants Exhibit Improved Sugar Release after Saccharification

The altered cell-wall composition and morphology of *uxs* triple mutants prompted us to examine the effect they might have on cell-wall digestibility. Consequently, the *uxs3 uxs5 uxs6* triple mutant showed improved glucose release of up to 18% compared with wild-type (Figure 6). Surprisingly, with lower xylose content, the *uxs3 uxs5 uxs6* triple mutant also showed increased release of xylose. The reason may be similar to what was observed in the *irx9* and transformant lines as shown by Petersen et al. (2012), which exhibited higher xylose released compared with the wild-type line. Xylan is more accessible to enzymatic breakdown in the *uxs3 uxs5 uxs6* triple mutant. The *uxs1 uxs2 uxs4* triple mutant showed no difference compared with the wild type, which was consistent with less change in the phenotype and monosaccharide composition.

DISCUSSION

Compartmentalization of AtUXS Enzymes

Comprehensive studies of gene expression provide useful information for predicting gene function. Previously, qPCR data illustrated that *Arabidopsis UXS* genes are mainly expressed in the stems, as are the xylan backbone and side-chain synthesis genes (Supplemental Figure 4) (Brown et al., 2009; Wu et al., 2009, 2010; Lee et al., 2010). Thus, the enhanced xylan deposition observed in stems could be supported by the increased level of UDP-Xyl produced by increased expression of *UXS* genes. AtUXS1, AtUXS2, and AtUXS4 (group II, Supplemental Figure 3) each have a type II membrane protein topology and are located in the Golgi lumen (Figure 1). In contrast, the second UXS clade that includes AtUXS3, AtUXS5, and AtUXS6 (group I) contain no predicted transmembrane domains and are located in the cytosol (Figure 1 and Supplemental Figure 5). The expression levels of group I members (AtUXS3, AtUXS5, and AtUXS6) in the stem are generally higher than the levels of group II members (AtUXS1,

	Wild-type (Col-0)	*uxs1 uxs2 uxs4*	*uxs3 uxs5 uxs6*
Fucose	0.97 ± 0.00	0.62 ± 0.01	0.79 ± 0.03
Rhamnose	4.05 ± 0.02	4.07 ± 0.03	5.93 ± 0.21
Arabinose	3.83 ± 0.03	3.45 ± 0.02	7.86 ± 0.26
Galactose	9.84 ± 0.05	9.51 ± 0.10	12.67 ± 0.30
Glucose	20.48 ± 0.03	19.12 ± 0.11	21.89 ± 0.64
Xylose	55.8 ± 0.05	58.34 ± 0.20	44.21 ± 0.48
GalA	4.45 ± 0.11	4.18 ± 0.06	6.32 ± 0.31
GlcA	0.57 ± 0.04	0.70 ± 0.06	0.33 ± 0.05

Table 1. Monosaccharide Composition, in mol%, of AIR from Cell-Wall Extracts of Stem Material from 6-Week-Old Plants.
Data represent mean ± SE (n = 3).

AtUXS2, and AtUXS4) (Supplemental Figure 4). This finding further highlights the potential importance of cytosolic-derived UDP-Xyl in cell-wall biosynthesis.

The cell-wall XylTs are located in the secretory pathway, mainly in the lumen of the Golgi apparatus, and are involved in the biosynthesis of xylan (IRX9, IRX10, IRX14 (Lee et al., 2012; Jensen et al., 2014)), xyloglucan (XXT1, XXT2, and XXT5 (Ahn et al., 2006)), and RG-II (RGXT1, RGXT2, RGXT3, and RGXT4 (Egelund et al., 2008; Liu et al., 2011)). The subcellular localization of these XylTs and the presence of Golgi-located UXS enzymes would indicate a central role for luminal UDP-Xyl. Recently, a family of three Golgi-located UXTs were characterized in *Arabidopsis* (Ebert et al., 2015). Moreover, *UXT1* mutant analysis indicated a reduction in cell-wall-derived Xyl from stem material and an apparent role in the biosynthesis of glucuronoxylans (Ebert et al., 2015). Thus, the transport of cytosolic UDP-Xyl into the Golgi lumen likely plays an essential role in providing substrates for xylan, and potentially xyloglucan and pectic polysaccharide biosynthetic enzymes (Figure 7).

Plant genomes and expressed sequence tag sequences reveal the diversity of *UXS* genes *in planta* (Supplemental Figure 1). Compared with other land plant genera, there are only two *UXS* genes in Norway spruce (*P. abies*). Based on sequence analysis, one UXS appears to be located in the cytosol and the other in the Golgi. This is possibly because heteromannans, not heteroxylans, are the major non-cellulosic polysaccharides in gymnosperms. A phylogenetic tree reveals that all UXS members in group I have no predicted transmembrane helices. However, in group II a majority of proteins have a predicted transmembrane helix except four members (EgUXS4, OsUXS2, OsUXS5, and HvUXS3). Interestingly, there is only one group I member in *P. patens*, barley, and rice, but in dicot species with well-developed vasculature such as *Arabidopsis*, *P. trichocarpa*, and *E. grandis*, there are multiple group I UXS members. This may be because these species require more cytosolic-synthesized UDP-Xyl for xylan biosynthesis. Further work is needed in *Arabidopsis* and other species to more precisely characterize the functions of the membrane-bound versus cytosolic UXS isoforms.

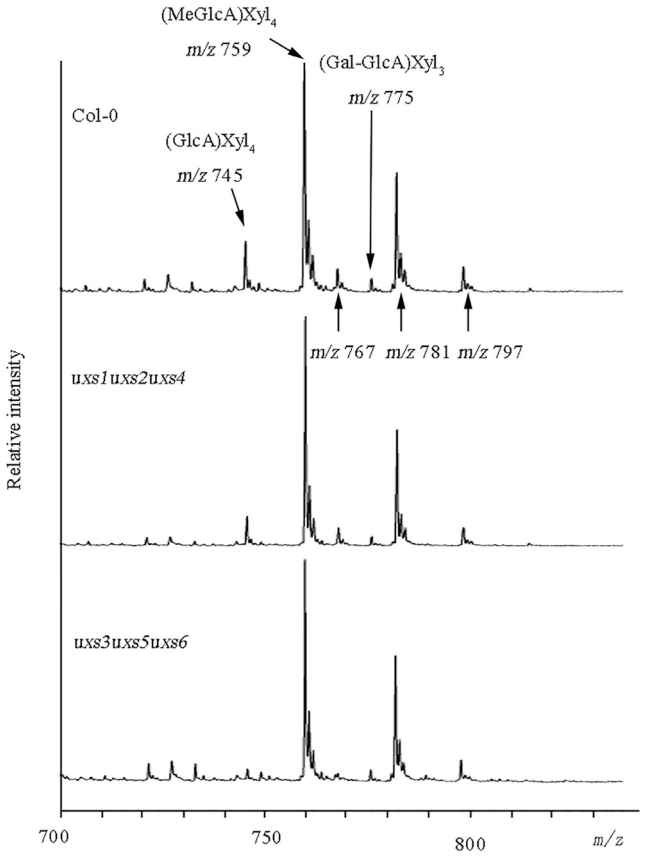

Figure 5. MALDI-TOF Mass Spectrum of Xylo-Oligomers from the wild-type Col-0, *uxs1 uxs2 uxs4*, and *uxs3 uxs5 uxs6* triple mutants.
The KOH extracted fraction from AIR of stem material was digested with an endo-xylanase and the resultant oligosaccharides analyzed by MALDI-TOF MS. The identity of prominent pseudo-molecular ion peaks (*m/z*) 745, 759, 767, 781, and 797 are attributed to (GlcA)Xyl_4-Na^+, (MeGlcA)Xyl_4-Na^+, (Gal-GlcA)Xyl_3-Na^+, (GlcA)Xyl_4-2Na^+, (MeGlcA)Xyl_4-2Na^+, and (Gal-GlcA)Xyl_3-2Na^+, respectively.

Cytosolic *UXS* Genes Are Redundant and Essential for Plant Development

The three cytosolic AtUXS enzymes (AtUXS3, AtUXS5, and AtUXS6) exhibited differential kinetic properties when expressed in *E. coli* with AtUXS3 showing the highest activity, as previously shown (Harper and Bar-Peled, 2002). In contrast, the luminal AtUXS enzymes (AtUXS1, AtUXS2, and AtUXS4) demonstrated a significant decrease in relative activity compared with the cytosolic isoforms when heterologously expressed in *N. benthamiana* (Figure 2A). These observations are similar to previous findings when comparing *in vitro* activities of the luminal isoforms AtUXS1 and AtUXS2 with AtUXS3 (Harper and Bar-Peled, 2002). A more recent analysis of AtUXS2 activity indicated that it has an apparent K_m of 0.2 mM, although this study was undertaken with an N-terminally truncated protein (Pattathil et al., 2005). Given the problems associated with assessing membrane-associated enzyme activities, it is unclear whether such distinct differences in activity between the cytosolic and luminal AtUXS enzymes exist.

	1 N KOH			2 N KOH		
	H_1	H_2	H_3	H_1	H_2	H_3
M_w	90 180	64 390	24 270	107 600	73 010	38 460
M_n	22 740	9795	9722	10 750	9102	10 020
M_w/M_n	3.97	6.57	2.50	10.01	8.02	3.84

Table 2. The Number-Average Molecular Weight M_n and Weight-Average Molecular Weight M_w (g/mol) of the Non-cellulosic Polysaccharides Extracted with 1 N KOH and 2 N KOH from Wild-Type (H_1), *uxs1 uxs2 uxs4* (H_2), and *uxs3 uxs5 uxs6* (H_3) Fractions.

While enzyme activities for *E. coli*-expressed AtUXS1, AtUXS2, and AtUXS3 have been previously reported (Harper and Bar-Peled, 2002; Pattathil et al., 2005), there are no reports on AtUXS enzyme function *in vivo*. Employing reverse genetics approaches, we found that single and double *uxs* mutants exhibit wild-type phenotypes, implying some level of functional redundancy (Supplemental Figure 9). As a consequence, we generated triple mutant lines based on the two functional AtUXS subgroups. The triple mutant, *uxs1 uxs2 uxs4* comprising group II members, resulted in no obvious phenotype. In contrast, the *uxs3 uxs5 uxs6* triple mutant comprising group I members resulted in a severe phenotype with delayed growth, darker leaf color, and a high proportion of irregular xylem vessels (Figures 3 and 4). This type of phenotype is very similar to the well-characterized xylan-defective mutants *irx7*, *irx8*, *irx9*, *irx10*, and *parvus* (Brown et al., 2009; Wu et al., 2009). These results indicated that collectively, the cytosolic AtUXS isoforms are likely more essential for the synthesis of xylan in stems. Finally, endogenous UXS activity in the triple mutants supported *in vitro* activity data, indicating that cytosolic AtUXS enzymes are more active than the luminal AtUXS enzymes.

While cytosolic AtUXS enzymes are likely to produce the majority of cytosolic UDP-Xyl, a cytosolic UDP-Api/UDP-Xyl synthase (AXS) also exists that is able to convert UDP-GlcA into both UDP-Xyl and UDP-Api (Figure 7) with an Api/Xyl ratio of 0.6 (Molhoj et al., 2003). These two *AtAXS* genes are highly expressed in all plant organs (Molhoj et al., 2003; Ahn et al., 2006) and are proposed to contribute to the assembly of RG-II side chains B and A, which contain D-Api (Ahn et al., 2006). Since Api is only present in the pectic polysaccharide RG-II (Stevenson et al., 1986), which is present in very low abundance, the amount of cytosolic UDP-Xyl produced by AXS is likely to be limited. Thus, the major pool of cytosolic UDP-Xyl is likely produced by UXS. This hypothesis is consistent with previous reports about *AXS* only affecting RG-II synthesis in tobacco (Ahn et al., 2006).

Lack of UXS Activity Leads to Altered Xylan

Employing chemical analyses and immunocytochemistry, we found that xylan derived from *Arabidopsis* stems was altered in abundance and molecular weight in the triple mutants when compared with wild-type (Tables 1, 2, and Supplemental Table 5). The xylan backbone synthesis genes *IRX9* and *IRX9-L*, *IRX14* and *IRX14-L*, and *IRX10* and *IRX10-L* are redundant pairs, with the "like" (-L) genes being minor isoforms (Brown et al., 2007, 2009; Lee et al., 2007; Peña et al., 2007;

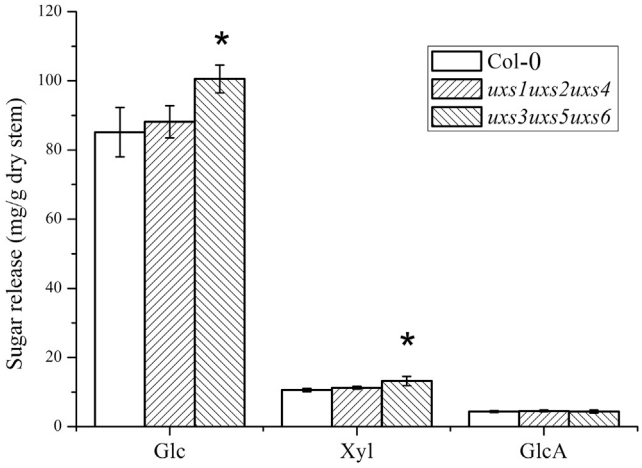

Figure 6. Saccharification Analyses.
Increased digestibility was observed in *uxs1 uxs2 uxs4* and *uxs3 uxs5 uxs6* triple mutant plants compared with the wild-type Col-0. Values show average ± SE (n = 5). *$p < 0.01$, significant difference from the wild type (*t*-test).

Keppler and Showalter, 2010; Wu et al., 2010; Chiniquy et al., 2013). This redundancy is linked to activity differences and suggests that xylan synthesis is dosage dependent and rate limited (Peña et al., 2007). UDP-Xyl is the main substrate for xylan synthesis, with Xyl residues constituting the entire backbone of this polysaccharide. We propose that UDP-Xyl concentration might decrease in *uxs* triple mutant plants and that this reduction in substrate availability for xylan biosynthesis results in reduced backbone elongation during fast growth of the stem. Although cytosolic-derived UDP-Xyl appears to be the main substrate source for xylan biosynthesis, the reduced molecular weight of xylan observed in the *uxs1 uxs2 uxs4* triple mutant also supports a contribution by luminal UXS to the UDP-Xyl pool for xylan biosynthesis. Thus, the reduced M_w of xylan in *uxs1 uxs2 uxs4* and *uxs3 uxs5 uxs6* indicates that the quantity of donor UDP-Xyl generated by both the Golgi and cytosolic UXS isoforms might be important in controlling xylan chain length.

The increased ratio of methylglucuronic acid (MeGlcA) to non-methylated GlcA is a common feature of all known xylan-deficient mutants (Zhong et al., 2005), a feature also observed in both the cytosolic and Golgi *UXS* triple mutant plants. 4-*O*-Methylation of GlcA is catalyzed by glucuronoxylan methyltransferase, which was classified as a DUF (domain of unknown function) 579 protein (Urbanowicz et al., 2012). In wild-type *Arabidopsis*, on average a side branch is added to one in eight Xyl residues with an Me-GlcA to GlcA ratio of 2 (Brown et al., 2007). Detailed analyses of xylan mutants indicated that while the proportion of non-methylated GlcA decreases, the overall amount of MeGlcA tends to remain the same (Ebert et al., 2015). These findings indicated that while xylan levels can be reduced, there is a requirement for a certain proportion of MeGlcA to be present in the cell wall.

Interestingly, IRX15 and IRX15L appear to affect xylan length, with the *irx15 irx15L* double mutant displaying enhanced saccharification capacity (Brown et al., 2011). Similar results were obtained with the triple mutants, *uxs1 uxs2 uxs4* and *uxs3*

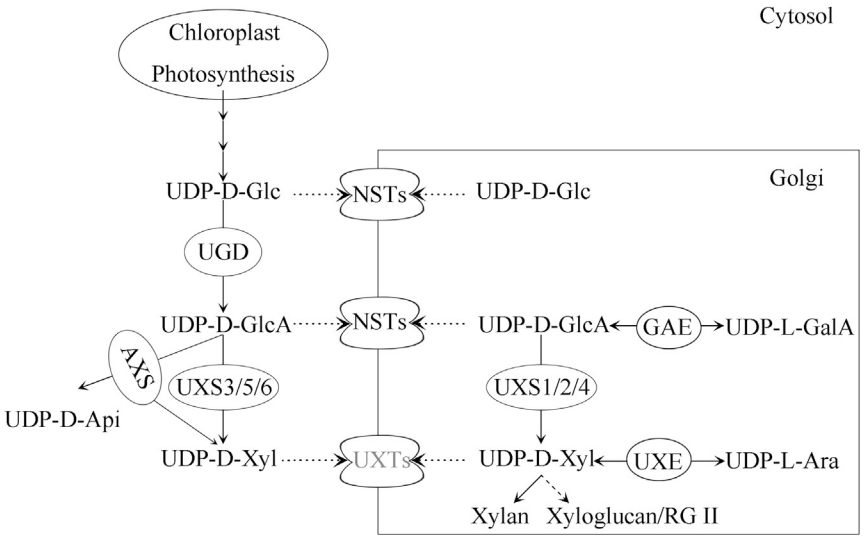

Figure 7. Overview of Metabolic Pathways and the Compartmentalization of Nucleotide Sugar Enzymes that Are Involved in UDP-D-Xyl Synthesis between the Cytosol and Golgi Lumen.

UGD, UDP-D-Glc dehydrogenase; GAE, UDP-GlcA epimerase; AXS, UDP-D-Api/UDP-D-Xyl synthase; UXE, UDP-D-Xyl 4-epimerase; UXS, UDP-glucuronic acid decarboxylase; NSTs, nucleotide sugar transporters; UXTs, UDP-Xyl transporters.

uxs5 uxs6 (Figure 6). Since xylan length contributes to recalcitrance of lignocellulosic biomass, it is possible that the lower DP (degree of polymerization) xylan would make the walls of the triple mutants more degradable.

METHODS

Phylogenetic and Sequence Analysis of *UXS* Genes

Amino acid sequences of the *UXS* genes were obtained from UniProt (UniProt Consortium, 2015). Sequence identities were determined using DNAMAN software version 8 (Lynnon Biosoft). Sequences were aligned using the Clustal MUSCLE program (Edgar, 2004) with default parameters. Phylogenetic trees were generated using the neighbor-joining method and bootstrap values generated from 1000 replicates. Prediction of transmembrane helices was conducted using TMHMM v.2.0 (Krogh et al., 2001).

Plant Growth Conditions

Seeds were surface sterilized in 10% NaOCl with 1% (v/v) Tween 20 (v/v), vortexed five times for 10 min, and washed three times in ultrapure water before 75% ethanol was added for 1 min, followed by three washes with sterilized water. Sterile seeds were sown on Murashige–Skoog medium plates (4.4 g of Murashige–Skoog basal salt mixture [pH 5.8] containing 1% [w/v] sucrose). The plates were refrigerated at 4°C in darkness for 2 days before transfer to a controlled environment growth cabinet (23°C, 60% humidity, 100–120 $\mu mol \cdot m^{-2} \cdot s^{-1}$, 16 h light/8 h dark). Seedlings were transferred to soil 10 days later for plant morphological analysis.

Plant Material and Identification of Homozygous Mutants

All *AtUXS* T-DNA insertion lines were obtained from the Arabidopsis Biological Resource Center (ABRC, https://abrc.osu.edu/) including *uxs1* (N555603, Salk_055603, sixth intron), *uxs2* (N503691, Salk_003691, first exon), *uxs3* (N907654, WiscDsLoxHs080_09, fifth exon), *uxs4* (N609630, Salk_109630, fifth intron), *uxs5* (N850623, WiscDsLox293-296invD4, eighth intron) and *uxs6* (N678548, salk_058602, second intron) (Figure 4A). The homozygous *uxs* combination mutants were obtained by genetic crosses. Homozygous T-DNA insertion mutants were identified by PCR of genomic DNA. Primers used for this purpose are listed in Supplemental Table 3.

Quantitative PCR Analysis

Total RNA of wild-type *Arabidopsis* was extracted with a plant total RNA extraction kit (Omega, USA) and treated with DNase I (Bio-Rad, USA). The first-strand cDNA was synthesized with a Takara cDNA synthesis kit (Cat. #6210, Takara, Japan) according to the manufacturer's protocol. Total RNA was extracted from 10-day-old shoots, 3-week-old rosette leaves, fully opened flowers, and 10-day-old siliques from 5-week-old plants, top, middle, and bottom parts of 7-week-old stems (in flower), and 2-week-old roots of wild-type plants. Primers for qPCR analysis were designed according to the *AtUXS* gene sequences, and only primer efficiencies for amplification were more than 92% listed for further analysis (Supplemental Table 2). Relative qPCR was performed according to the method of Schmittgen and Livak (2008).

Transcript Analysis by RT–PCR

For determination of *UXS* gene expression, total RNA from 2-week-old seedlings in *uxs* mutants and wild-type were extracted and treated using the methods listed above. The *AtUXS* transcripts were analyzed by PCR using the primers as listed in Supplemental Table 4. PCR included an initial heating step (5 min, 94°C), followed by 36 cycles consisting of denaturation (25 s, 94°C), annealing (25 s, 55°C), and extension (50 s, 72°C), and a final incubation at 72°C for 10 min. PCR products were separated on a 2% (w/v) agarose gel in TAE (Tris/acetate/EDTA) buffer. As a control, the 18s RNA was amplified for 24 cycles (for primers see Supplemental Table 4).

Stem Sectioning

Stem segments were cut at a height of 3 cm from the rosette of 8-week-old soil-grown plants with full siliques and then embedded in 3% (w/v) agarose (BioWest, Spain). Sections (50 μm) were then cut with a VT1000S vibratome (Leica, Germany). The sections were stained with 0.02% toluidine blue O (Sigma-Aldrich) for 30 s to 1 min, washed with water, and observed under a light microscope (Olympus BX43F, Japan). Stem segments from three independent plants were collected, and >10 sections were viewed per plant.

Transmission Electron Microscopy

Stem segments were cut from the bottom part of 8-week-old soil-grown plants with full siliques and then vacuum infiltrated in 4% (v/v) glutaraldehyde in PBS (33 mM Na_2HPO_4, 1.8 mM NaH_2PO_4, and 140 mM NaCl [pH 7.2]) before being fixed in 2% glutaraldehyde in PBS at 4°C overnight. After fixation, tissues were post-fixed in 1% (w/v) osmium tetroxide, then dehydrated through a gradient of ethanol and embedded in Spurr's resin. Sections (70–100 nm) were stained with uranyl acetate and lead citrate and visualized using an FEI Tecnai 12 transmission electron microscope. Finally, cell-wall thickness was measured from eight cells on each section with three technical repeats using FEI microscopy software DigitalMicrograph (Gatan).

Immunolocalization Analysis of Heteroxylans in Mutants

Sections were washed with 0.1 M PBS buffer (0.1 M PBS, 0.5 M NaCl [pH 7.2]), then incubated with 3% (w/v) skim milk powder in PBS for 2 h. LM10,

which can bind to unsubstituted and relatively low-substituted heteroxylans but not to wheat arabinoxylan (McCartney et al., 2005), was diluted 1/20 with 0.1 M PBS buffer and incubated for 4 h at room temperature. Sections were then washed with PBS buffer (five times) before secondary antibody (fluorescein isothiocyanate-conjugated, 1/50 dilution; Abcam, http://www.Abcam.com) was added. After incubation for 1 h at room temperature the sections were washed a further five times and the immunofluorescence observed on a Zeiss LSM710 confocal microscope.

Subcellular Location of AtUXS

Gateway primers (Supplemental Table 6) containing *attB* site were designed for amplification of *AtUXS* genes. The PCR products without stop codons were cloned into the pDONR207 vector by BP reaction (Life Technologies, USA) and sequenced. Verified clones were transferred into the pEarleyGate 101 destination vector (Earley et al., 2006) to produce the C-terminal YFP fusion constructs. Each of the pEarlyGate101-*AtUXS* constructs were transformed into *Agrobacterium tumefaciens* strain C58. pEarlyGate101-*AtUXS* in C58 were infiltrated into *Nicotiana benthamina* as previously described (Sparkes et al., 2006). YFP signal was observed under an excitation wavelength of 514 nm and an emission wavelength of 510–545 nm. The *AtUXS3*, *AtUXS5*, and *AtUXS6* constructs were co-infiltrated with the soybean α-mannosidase-mCherry (G-rb CD3-968) Golgi marker (Nelson et al., 2007), which was visualized using excitation wavelength of 587 nm and emission wavelength 610 nm, to verify the location of the three proteins.

Expression of Soluble AtUXS3, AtUXS5, and AtUXS6 in *E. coli*

Cytosolic *AtUXS* genes were cloned into pGEX-4T by digestion and ligation at *Xho*I and *Eco*RI sites with primers listed in Supplemental Table 6 and confirmed by sequencing. pET-4X-*AtUXS* constructs were introduced into *E. coli* strain BL21 via electroporation. Cultures were grown at 37°C to OD_{600} = 0.6 and isopropyl β-D-1-thiogalactopyranoside added to a final concentration of 0.5 mM. After 3 h of induction, the cells were pelleted by centrifugation at 6000 *g* for 10 min and 4°C, and resuspended in 10 ml of extraction buffer (50 mM Tris–HCl [pH 7.4], 10% glycerol, 1 mM EDTA) with fresh 1 mM DTT and 0.5 mM PMSF. The solution was lysed by sonication using a 10-s pulse followed by 20 s rest on ice, then collected, and the proteins purified as previously described (Bar-Peled and Raikhel, 1996). Finally, purified protein was centrifuged in an Amicon-Ultra-15 filter (MWCO10KD) at 4°C and 4000 *g* for 45 min and filtered twice with Tris–HCl (pH 7.4) buffer. Protein content was calculated with the Bradford protein assay (Bio-Rad, USA).

Western Blotting Analysis

The purified GST-UXS5 protein was collected and injected into three rabbits to obtain optimized polyclonal antibodies at Beijing Protein Innovation (www.proteomics.org.cn/). pEarlyGate101-*AtUXS* in C58 was infiltrated into *N. benthamiana* as previously described (Sparkes et al., 2006). Western blotting was performed essentially as previously described (Tamura et al., 2005). The tobacco leaves were excised and ground on ice in 3 ml of 20 mM Tris–HCl (pH 7.4) buffer with proteinase inhibitor cocktail (Roche, Switzerland). The homogenate was filtered using cheesecloth and centrifuged at 4000 *g* for 30 min at 4°C to remove cellular debris. The supernatant, including soluble proteins and microsomal proteins, was used for western blotting and to measure enzyme activity. In western blotting, the protein extract buffer included 2% Triton X-100. The total protein extracts were: 80 μg loaded in lanes of AtUXS3, AtUXS5, AtUXS6; and 160 μg loaded in lanes of UXS1, UXS2, and UXS4. The anti-UXS5 polyclonal antibodies were used to detect UXS3, UXS5, and UXS6 (1:100 dilution), but do not detect the membrane-bound UXS isoforms. The anti-HA antibody (Sigma-Aldrich, USA) was used to detect UXS1, UXS2, and UXS4 at 1:1000 dilution. Blots were washed and then incubated with anti-mouse immunoglobulin G coupled to alkaline phosphatase (Sigma-Aldrich, USA) at a dilution of 1:5000 and developed according to the manufacturer's instructions.

AtUXS Activity Assays

AtUXS activity assays were performed as previously described (Bar-Peled et al., 2001; Zhao et al., 2014). In brief, 50 μl of standard reaction mixture containing 80 mM Tris–HCl (pH 7.4), 1 mM NAD^+, 1 mM UDP-GlcA, and 10 μg of protein were incubated at 25°C for 2 h. Reactions were terminated by the addition of 50 μl of phenol/chloroform (1:1, v/v), vortex-mixed, and subjected to centrifugation (10 000 *g*, 5 min). The upper phase was retained and 100 μl of ultrapure water added to re-extract the lower phase. The upper phases were mixed and analyzed by HPLC using a COSMOSIL C18-AR-II column (4.6 × 250 mm; Nacalai Tesque, Kyoto, Japan) run at 1 ml min^{-1} and monitored for UV absorbance (Agilent 1100 HPLC systems, Sig_{260nm}, Ref_{360nm}). Buffer A contained 20 mM triethylamine acetate (pH 7) and buffer B contained 20 mM triethylamine acetate mixed with 10% (v/v) acetonitrile. The gradient was 0–15 min (0% B), 15.1–30 min (15% B), and post-run time 5 min (Rosenberger et al., 2012).

Cell-Wall Extraction and Linkage Analysis

The bottom section of stems (5 cm length from base) of 8-week-old (with maturing siliques) wild-type and *uxs1 uxs2 uxs4* and *uxs3 uxs5 uxs6* triple mutants, were collected and ground with a mortar and pestle in liquid N_2. AIR was prepared by extraction of the powder with 96% (v/v) ethanol at 70°C for 30 min, and the insoluble fraction used for measurement of both neutral and acidic monosaccharide linkage composition as previously described (Pettolino et al., 2012).

Gel-Permeation Chromatography of Non-cellulosic Polysaccharides

Non-cellulosic polysaccharides were sequentially extracted from AIR samples (outlined above) with 1 N and 2 N KOH at 50°C for 3 h. The KOH extracts were neutralized with acetic acid to pH 5.5 and then precipitated in three volumes of 95% ethanol. The precipitates were collected by centrifuging at 3000 *g* for 5 min, washed with acidified 70% ethanol, and freeze-dried. The molecular weight was determined by gel-permeation chromatography–multi angle laser light scattering (GPC-MALLS) methods. GPC-MALLS measurements were carried out on a DAWN HELEOS-II laser photometer (Wyatt Technology, USA), combined with a PL Aquagel-OH 50 column (300 × 7.7 mm, Polymer Laboratories, USA) at 45°C equipped with a Model 600 pump HPLC system (Waters, USA) and an Optilab rEX differential refractive index detector (Wyatt Technology). The eluent was 0.02 N NaCl in 0.005 M sodium phosphate buffer (pH 7.5) with a flow rate of 0.5 ml min^{-1}. Non-cellulosic polysaccharides were dissolved with the eluent buffer at a concentration of 1.0 mg ml^{-1} and filtered using a 0.42-μm microfiltration membrane.

Determination of Monosaccharide Composition

AIR was extracted from stem material (as outlined above) and hydrolyzed in 2 N trifluoroacetic acid for 1 h at 120°C according to previous methods (Ebert et al., 2015). Sugars were separated and quantified by high-performance anion exchange chromatography with pulsed amperometric detection as described by Øbro et al. (2004) on an ICS 3000 (Dionex) using a CarboPac PA1 anion exchange column (3 × 150 mm; Dionex).

MALDI-TOF MS

MALDI-TOF MS was performed on KOH extracts (as outlined above) and analyzed as described by Zhong et al. (2005). Xylan oligosaccharides were generated by *endo*-β-xylanase M6 (Megazyme) digestion, then analyzed by MALDI-TOF MS with a Bruker microFLEX MALDI-TOF MS operated in the positive-ion mode with an accelerating voltage of 30 kV, an extractor voltage of 9 kV, and a source pressure of about 8×10^{-7} torr. The matrix was prepared by mixing saturated 2,5-dihydroxybenzoic acid in 50% aqueous acetonitrile. The typical spectra shown represents the sums of 200 laser shots. MeGlcA content was calculated by the peak areas of ((MeGlcA)-Xyl_4 and (MeGlcA)-Xyl_4)/total (GlcA)-Xyl_4.

Saccharification

A 6-cm piece from the base of the stems of 8-week-old *Arabidopsis* were collected and ground using a PM100 Ball Mill (Retsch, Germany). Saccharification was undertaken following cell-wall pretreatment by autoclaving for 30 min at 120°C and using the modified procedure of Petersen et al. (2012). For enzymatic saccharification, a mixture of 5 mg/ml tetracycline and 2 mg/ml mixed cellulase containing β-glucanase (3.7×10^4 U), cellulase (3.4×10^2 U), and xylanase (6.5×10^4 U) (Imperial Jade Bio-Technology, China) in 0.1 M citrate buffer (pH 5.0) was added to the pretreated samples, followed by incubation at 50°C for 24 h at 100 rpm. The monosaccharide products were determined by HPLC using an SP-0810 Shodex SUGAR column coupled to a refractive index detector. Degradation products were detected using a UV detector (Yu et al., 2010).

SUPPLEMENTAL INFORMATION

Supplemental Information is available at *Molecular Plant Online*.

FUNDING

This work was supported by the Science and Technology Planning Project of Guangdong Province (grant number 2015A050502045), National Natural Science Foundation of China (grant numbers 31170165 and 31270594), Ministry of Science and Technology of China (grant numbers 2013AA102705, 2013BAD22B01), Guangdong Natural Science foundation (grant number S2013010011988), the Taishan Scholar Program of Shandong (G. Z.), and ARC Center of Excellence in Plant Cell Walls, Australia (grant number CE110001007).

AUTHOR CONTRIBUTIONS

K.B., C.X., and W.A. designed research; K.B., Z.X., Z.C., Z.W., R.J., E.B., B.C.T., D.X., Z Q., and Z.G. performed research; D.M.S., H.J.L., B.A., C.X., and W.A. analyzed data; K.B., B.A., and W.A. wrote the paper.

ACKNOWLEDGMENTS

We thank Jing Fan, Chunxu Ni, and Haoyang Fu for their help in protein expression in *E. coli*. All pEarlyGate vectors, Golgi marker (CD3-968), and *Arabidopsis uxs* mutants were provided by ABRC at Ohio State University (www.arabidopsis.org). C.B., W.Z., M.S.D., and A.B. acknowledge support of the ARC Center of Excellence in Plant Cell Walls. No conflict of interest declared.

Received: January 27, 2016
Revised: April 18, 2016
Accepted: April 26, 2016
Published: May 11, 2016

REFERENCES

Ahn, J.W., Verma, R., Kim, M., Lee, J.Y., Kim, Y.K., Bang, J.W., Reiter, W.D., and Pai, H.S. (2006). Depletion of UDP-D-apiose/UDP-D-xylose synthases results in rhamnogalacturonan-II deficiency, cell wall thickening, and cell death in higher plants. J. Biol. Chem. **281**:13708–13716.

Bar-Peled, M., and O'Neill, M.A. (2011). Plant nucleotide sugar formation, interconversion, and salvage by sugar recycling. Annu. Rev. Plant Biol. **62**:127–155.

Bar-Peled, M., and Raikhel, N.V. (1996). A method for isolation and purification of specific antibodies to a protein fused to the GST. Anal. Biochem. **241**:140–142.

Bar-Peled, M., Griffith, C.L., and Doering, T.L. (2001). Functional cloning and characterization of a UDP- glucuronic acid decarboxylase: the pathogenic fungus *Cryptococcus neoformans* elucidates UDP-xylose synthesis. Proc. Natl. Acad. Sci. USA **98**:12003–12008.

Bindschedler, L.V., Tuerck, J., Maunders, M., Ruel, K., Petit-Conil, M., Danoun, S., Boudet, A.M., Joseleau, J.P., and Bolwell, G.P. (2007). Modification of hemicellulose content by antisense down-regulation of UDP-glucuronate decarboxylase in tobacco and its consequences for cellulose extractability. Phytochemistry **68**:2635–2648.

Brown, D.M., Zeef, L.A., Ellis, J., Goodacre, R., and Turner, S.R. (2005). Identification of novel genes in *Arabidopsis* involved in secondary cell wall formation using expression profiling and reverse genetics. Plant Cell **17**:2281–2295.

Brown, D.M., Goubet, F., Wong, V.W., Goodacre, R., Stephens, E., Dupree, P., and Turner, S.R. (2007). Comparison of five xylan synthesis mutants reveals new insight into the mechanisms of xylan synthesis. Plant J. **52**:1154–1168.

Brown, D.M., Zhang, Z., Stephens, E., Dupree, P., and Turner, S.R. (2009). Characterization of IRX10 and IRX10-like reveals an essential role in glucuronoxylan biosynthesis in *Arabidopsis*. Plant J. **57**:732–746.

Brown, D., Wightman, R., Zhang, Z., Gomez, L.D., Atanassov, I., Bukowski, J.P., Tryfona, T., McQueen-Mason, S.J., Dupree, P., and Turner, S. (2011). Arabidopsis genes IRREGULAR XYLEM (IRX15) and IRX15L encode DUF579-containing proteins that are essential for normal xylan deposition in the secondary cell wall. Plant J. **66**:401–413.

Cavalier, D.M., and Keegstra, K. (2006). Two xyloglucan xylosyltransferases catalyze the addition of multiple xylosyl residues to cellohexaose. J. Biol. Chem. **281**:34197–34207.

Cavalier, D.M., Lerouxel, O., Neumetzler, L., Yamauchi, K., Reinecke, A., Freshour, G., Zabotina, O.A., Hahn, M.G., Burgert, I., Pauly, M., et al. (2008). Disrupting two *Arabidopsis thaliana* xylosyltransferase genes results in plants deficient in xyloglucan, a major primary cell wall component. Plant Cell **20**:1519–1537.

Chiniquy, D., Varanasi, P., Oh, T., Harholt, J., Katnelson, J., Singh, S., Auer, M., Simmons, B., Adams, P.D., Scheller, H.V., et al. (2013). Three novel rice genes closely related to the *Arabidopsis* IRX9, IRX9L, and IRX14 genes and their roles in xylan biosynthesis. Front. Plant Sci. **4**:83.

Doblin, M.S., Pettolino, F., and Bacic, A. (2010). Plant cell walls: the skeleton of the plant world. Funct. Plant Biol. **37**:357–381.

Doblin, M.S., Johnson, K.L., Humphries, J., Newbigin, E.J., and Bacic, A. (2014). Are designer plant cell walls a realistic aspiration or will the plasticity of the plant's metabolism win out? Curr. Opin. Biotechnol. **26**:108–114.

Du, Q., Pan, W., Tian, J., Li, B., and Zhang, D. (2013). The UDP-glucuronate decarboxylase gene family in Populus: structure, expression, and association genetics. PLoS One **8**:e60880.

Earley, K.W., Haag, J.R., Pontes, O., Opper, K., Juehne, T., Song, K., and Pikaard, C.S. (2006). Gateway-compatible vectors for plant functional genomics and proteomics. Plant J. **45**:616–629.

Ebert, B., Rautengarten, C., Guo, X., Xiong, G., Stonebloom, S., Smith-Moritz, A.M., Herter, T., Chan, L.J., Adams, P.D., Petzold, C.J., et al. (2015). Identification and characterization of a Golgi-localized UDP-xylose transporter family from *Arabidopsis*. Plant Cell **27**:1218–1227.

Edgar, R.C. (2004). MUSCLE: a multiple sequence alignment method with reduced time and space complexity. BMC Bioinformatics **5**:113.

Egelund, J., Petersen, B.L., Motawia, M.S., Damager, I., Faik, A., Olsen, C.E., Ishii, T., Clausen, H., Ulvskov, P., and Geshi, N. (2006). *Arabidopsis thaliana* RGXT1 and RGXT2 encode Golgi-localized (1,3)-alpha-D-xylosyltransferases involved in the synthesis of pectic rhamnogalacturonan-II. Plant Cell **18**:2593–2607.

Egelund, J., Damager, I., Faber, K., Olsen, C.E., Ulvskov, P., and Petersen, B.L. (2008). Functional characterisation of a putative rhamnogalacturonan II specific xylosyltransferase. FEBS Lett. **582**:3217–3222.

Gotting, C., Kuhn, J., Zahn, R., Brinkmann, T., and Kleesiek, K. (2000). Molecular cloning and expression of human UDP-d-Xylose: proteoglycan core protein beta-d-xylosyltransferase and its first isoform XT-II. J. Mol. Biol. **304**:517–528.

Harper, A.D., and Bar-Peled, M. (2002). Biosynthesis of UDP-xylose. Cloning and characterization of a novel *Arabidopsis* gene family, UXS, encoding soluble and putative membrane-bound UDP-glucuronic acid decarboxylase isoforms. Plant Physiol. **130**:2188–2198.

Hayashi, T., Koyama, T., and Matsuda, K. (1988). Formation of UDP-xylose and xyloglucan in soybean Golgi membranes. Plant Physiol. **87**:341–345.

Jensen, J.K., Sorensen, S.O., Harholt, J., Geshi, N., Sakuragi, Y., Moller, I., Zandleven, J., Bernal, A.J., Jensen, N.B., Sorensen, C., et al. (2008). Identification of a xylogalacturonan xylosyltransferase involved in pectin biosynthesis in *Arabidopsis*. Plant Cell **20**:1289–1302.

Jensen, J.K., Johnson, N.R., and Wilkerson, C.G. (2014). *Arabidopsis thaliana* IRX10 and two related proteins from psyllium and *Physcomitrella patens* are xylan xylosyltransferases. Plant J. **80**:207–215.

Keppler, B.D., and Showalter, A.M. (2010). IRX14 and IRX14-LIKE, two glycosyl transferases involved in glucuronoxylan biosynthesis and drought tolerance in *Arabidopsis*. Mol. Plant **3**:834–841.

Kobayashi, M., Nakagawa, H., Suda, I., Miyagawa, I., and Matoh, T. (2002). Purification and cDNA cloning of UDP-D-glucuronate carboxy-lyase (UDP-D-xylose synthase) from pea seedlings. Plant Cell Physiol. **43**:1259–1265.

Krogh, A., Larsson, B., von Heijne, G., and Sonnhammer, E.L.L. (2001). Predicting transmembrane protein topology with a hidden Markov model: application to complete genomes. J. Mol. Biol. **305**:567–580.

Lee, C., O'Neill, M.A., Tsumuraya, Y., Darvill, A.G., and Ye, Z.H. (2007). The irregular xylem9 mutant is deficient in xylan xylosyltransferase activity. Plant Cell Physiol. **48**:1624–1634.

Lee, C., Teng, Q., Huang, W., Zhong, R., and Ye, Z.H. (2010). The *Arabidopsis* family GT43 glycosyltransferases form two functionally nonredundant groups essential for the elongation of glucuronoxylan backbone. Plant Physiol. **153**:526–541.

Lee, C., Zhong, R., and Ye, Z.H. (2012). *Arabidopsis* family GT43 members are xylan xylosyltransferases required for the elongation of the xylan backbone. Plant Cell Physiol. **53**:135–143.

Liu, X.L., Liu, L., Niu, Q.K., Xia, C., Yang, K.Z., Li, R., Chen, L.Q., Zhang, X.Q., Zhou, Y., and Ye, D. (2011). Male gametophyte defective 4 encodes a rhamnogalacturonan II xylosyltransferase and is important for growth of pollen tubes and roots in *Arabidopsis*. Plant J. **65**:647–660.

McCartney, L., Marcus, S.E., and Knox, J.P. (2005). Monoclonal antibodies to plant cell wall xylans and arabinoxylans. J. Histochem. Cytochem. **53**:543–546.

Molhoj, M., Verma, R., and Reiter, W.D. (2003). The biosynthesis of the branched-chain sugar d-apiose in plants: functional cloning and characterization of a UDP-d-apiose/UDP-d-xylose synthase from *Arabidopsis*. Plant J. **35**:693–703.

Nelson, B.K., Cai, X., and Nebenfuhr, A. (2007). A multicolored set of in vivo organelle markers for co-localization studies in *Arabidopsis* and other plants. Plant J. **51**:1126–1136.

Øbro, J., Harholt, J., Scheller, H.V., and Orfila, C. (2004). Rhamnogalacturonan I in *Solanum tuberosum* tubers contains complex arabinogalactan structures. Phytochemistry **65**:1429–1438.

Okazawa, K., Sato, Y., Nakagawa, T., Asada, K., Kato, I., Tomita, E., and Nishitani, K. (1993). Molecular cloning and cDNA sequencing of endoxyloglucan transferase, a novel class of glycosyltransferase that mediates molecular grafting between matrix polysaccharides in plant cell walls. J. Biol. Chem. **268**:25364–25368.

Pattathil, S., Harper, A.D., and Bar-Peled, M. (2005). Biosynthesis of UDP-xylose: characterization of membrane-bound AtUxs2. Planta **221**:538–548.

Pauly, M., and Keegstra, K. (2010). Plant cell wall polymers as precursors for biofuels. Curr. Opin. Plant Biol. **13**:305–312.

Peña, M.J., Zhong, R., Zhou, G.K., Richardson, E.A., O'Neill, M.A., Darvill, A.G., York, W.S., and Ye, Z.H. (2007). *Arabidopsis* irregular xylem8 and irregular xylem9: implications for the complexity of glucuronoxylan biosynthesis. Plant Cell **19**:549–563.

Petersen, P.D., Lau, J., Ebert, B., Yang, F., Verhertbruggen, Y., Kim, J.S., Varanasi, P., Suttangkakul, A., Auer, M., Loque, D., et al. (2012). Engineering of plants with improved properties as biofuels feedstocks by vessel-specific complementation of xylan biosynthesis mutants. Biotechnol. Biofuels **5**:84.

Pettolino, F.A., Walsh, C., Fincher, G.B., and Bacic, A. (2012). Determining the polysaccharide composition of plant cell walls. Nat. Protoc. **7**:1590–1607.

Ray, P.M. (1980). Cooperative action of beta-glucan synthetase and UDP-xylose xylosyl transferase of Golgi membranes in the synthesis of xyloglucan-like polysaccharide. Biochim. Biophys. Acta **629**:431–444.

Reiter, W.D. (2008). Biochemical genetics of nucleotide sugar interconversion reactions. Curr. Opin. Plant Biol. **11**:236–243.

Reiter, W.D., and Vanzin, G.F. (2001). Molecular genetics of nucleotide sugar interconversion pathways in plants. Plant Mol. Biol. **47**:95–113.

Rodgers, M.W., and Bolwell, G.P. (1992). Partial purification of Golgi-bound arabinosyltransferase and two isoforms of xylosyltransferase from French bean (*Phaseolus vulgaris* L.). Biochem. J. **288**:817–822.

Rosenberger, A.F., Hangelmann, L., Hofinger, A., and Wilson, I.B. (2012). UDP-xylose and UDP-galactose synthesis in *Trichomonas vaginalis*. Mol. Biochem. Parasitol. **181**:53–56.

Schmittgen, T.D., and Livak, K.J. (2008). Analyzing real-time PCR data by the comparative C(T) method. Nat. Protoc. **3**:1101–1108.

Seifert, G.J. (2004). Nucleotide sugar interconversions and cell wall biosynthesis: how to bring the inside to the outside. Curr. Opin. Plant Biol. **7**:277–284.

Sparkes, I.A., Runions, J., Kearns, A., and Hawes, C. (2006). Rapid, transient expression of fluorescent fusion proteins in tobacco plants and generation of stably transformed plants. Nat. Protoc. **1**:2019–2025.

Stevenson, T.T., McNeil, M., Darvill, A.G., and Albersheim, P. (1986). Structure of plant cell walls: XVIII. An analysis of the extracellular polysaccharides of suspension-cultured sycamore cells. Plant Physiol. **80**:1012–1019.

Strasser, R., Mucha, J., Mach, L., Altmann, F., Wilson, I.B., Glossl, J., and Steinkellner, H. (2000). Molecular cloning and functional expression of beta1, 2-xylosyltransferase cDNA from *Arabidopsis thaliana*. FEBS Lett. **472**:105–108.

Suzuki, K., Suzuki, Y., and Kitamura, S. (2003). Cloning and expression of a UDP-glucuronic acid decarboxylase gene in rice. J. Exp. Bot. **54**:1997–1999.

Suzuki, K., Watanabe, K., Masumura, T., and Kitamura, S. (2004). Characterization of soluble and putative membrane-bound UDP-glucuronic acid decarboxylase (OsUXS) isoforms in rice. Arch. Biochem. Biophys. **431**:169–177.

Tamura, K., Shimada, T., Kondo, M., Nishimura, M., and Hara-Nishimura, I. (2005). KATAMARI1/MURUS3 Is a novel Golgi membrane protein that is required for endomembrane organization in *Arabidopsis*. Plant Cell **17**:1764–1776.

UniProt Consortium. (2015). UniProt: a hub for protein information. Nucleic Acids Res. **43**:D204–D212.

Urbanowicz, B.R., Pena, M.J., Ratnaparkhe, S., Avci, U., Backe, J., Steet, H.F., Foston, M., Li, H., O'Neill, M.A., Ragauskas, A.J., et al. (2012). 4-O-methylation of glucuronic acid in *Arabidopsis* glucuronoxylan is catalyzed by a domain of unknown function family 579 protein. Proc. Natl. Acad. Sci. USA **109**:14253–14258.

Urbanowicz, B.R., Pena, M.J., Moniz, H.A., Moremen, K.W., and York, W.S. (2014). Two *Arabidopsis* proteins synthesize acetylated xylan in vitro. Plant J. **80**:197–206.

Wierenga, R.K., Terpstra, P., and Hol, W.G. (1986). Prediction of the occurrence of the ADP-binding beta alpha beta-fold in proteins, using an amino acid sequence fingerprint. J. Mol. Biol. **187**:101–107.

Winter, D., Vinegar, B., Nahal, H., Ammar, R., Wilson, G.V., and Provart, N.J. (2007). An "Electronic Fluorescent Pictograph" browser for exploring and analyzing large-scale biological data sets. PLoS One **2**:e718.

Wu, A.M., Rihouey, C., Seveno, M., Hornblad, E., Singh, S.K., Matsunaga, T., Ishii, T., Lerouge, P., and Marchant, A. (2009). The *Arabidopsis* IRX10 and IRX10-LIKE glycosyltransferases are critical for glucuronoxylan biosynthesis during secondary cell wall formation. Plant J. **57**:718–731.

Wu, A.M., Hornblad, E., Voxeur, A., Gerber, L., Rihouey, C., Lerouge, P., and Marchant, A. (2010). Analysis of the *Arabidopsis* IRX9/IRX9-L and IRX14/IRX14-L pairs of glycosyltransferase genes reveals critical contributions to biosynthesis of the hemicellulose glucuronoxylan. Plant Physiol. **153**:542–554.

Yu, Q., Zhuang, X., Yuan, Z., Wang, Q., Qi, W., Wang, W., Zhang, Y., Xu, J., and Xu, H. (2010). Two-step liquid hot water pretreatment of *Eucalyptus grandis* to enhance sugar recovery and enzymatic digestibility of cellulose. Bioresour. Technol. **101**:4895–4899.

Zabotina, O.A., van de Ven, W.T., Freshour, G., Drakakaki, G., Cavalier, D., Mouille, G., Hahn, M.G., Keegstra, K., and Raikhel, N.V. (2008). *Arabidopsis* XXT5 gene encodes a putative alpha-1,6-xylosyltransferase that is involved in xyloglucan biosynthesis. Plant J. **56**:101–115.

Zhang, Q., Shirley, N., Lahnstein, J., and Fincher, G.B. (2005). Characterization and expression patterns of UDP-D-glucuronate decarboxylase genes in barley. Plant Physiol. **138**:131–141.

Zhao, X., Ouyang, K., Gan, S., Zeng, W., Song, L., Zhao, S., Li, J., Doblin, M.S., Bacic, A., Chen, X.Y., et al. (2014). Biochemical and molecular changes associated with heteroxylan biosynthesis in *Neolamarckia cadamba* (Rubiaceae) during xylogenesis. Front. Plant Sci. **5**:602.

Zhong, R., Pena, M.J., Zhou, G.K., Nairn, C.J., Wood-Jones, A., Richardson, E.A., Morrison, W.H., 3rd, Darvill, A.G., York, W.S., and Ye, Z.H. (2005). *Arabidopsis* fragile fiber8, which encodes a putative glucuronyltransferase, is essential for normal secondary wall synthesis. Plant Cell **17**:3390–3408.

Zhong, R., Teng, Q., Lee, C., and Ye, Z.H. (2014). Identification of a disaccharide side chain 2-O-alpha-D-galactopyranosyl-alpha-D-glucuronic acid in *Arabidopsis* xylan. Plant Signal. Behav. **9**:e27933.